

# Inhomogeneous states with checkerboard order in the $t$ - $J$ Model

Chunhua Li, Sen Zhou, and Ziqiang Wang

*Department of Physics, Boston College, Chestnut Hill, MA 02467, USA*

(Dated: March 23, 2022)

We study inhomogeneous states in the  $t$ - $J$  model using an unrestricted Gutzwiller approximation. We find that  $pa \times pa$  checkerboard order, where  $p$  is a doping dependent number, emerges from Fermi surface instabilities of both the staggered flux phase and the Fermi liquid state with realistic band parameters. In both cases, the checkerboard order develops at wave vectors  $(\pm 2\pi/pa, 0)$ ,  $(0, \pm 2\pi/pa)$  that are tied to the peaks of the wave-vector dependent susceptibility, and is of the Lomer-Rice-Scott type. The properties of such periodic, inhomogeneous states are discussed in connection to the checkerboard patterns observed by STM in underdoped cuprates.

Spatially inhomogeneous, periodically modulated local density of states (LDOS) has been observed recently by STM in high- $T_c$  cuprates under a variety of conditions where the superconductivity is weakened<sup>1,2,3,4,5</sup>. The hope for a certain type of ordered state competing with superconductivity has been raised in connection to the pseudogap phenomena. The tunneling conductance map exhibits  $pa \times pa$  checkerboard (CB) patterns corresponding to wave vectors  $(\pm 2\pi/p, 0)$ ,  $(0, \pm 2\pi/p)$ , where  $p$  takes on values between 4 and 5 (hereafter, we set the lattice constant  $a = 1$ ). In and around a vortex core in  $\text{Bi}_2\text{Sr}_2\text{CaCu}_2\text{O}_{8+\delta}$  (BSCCO),  $p \sim 4.3$ <sup>1</sup>;  $p \sim 4$  in optimally doped BSCCO in zero magnetic field<sup>2</sup>;  $p \simeq 4.7$  in underdoped BSCCO in the pseudogap phase above  $T_c$ <sup>3</sup>;  $p \simeq 4$  in lightly doped oxchlorides  $\text{Ca}_{2-x}\text{Na}_x\text{CuO}_2\text{Cl}_2$  (Na-CCOC) at very low temperatures<sup>4</sup>; and in substantially underdoped BSCCO,  $p \sim 4.5$  were observed in the dark regions of the conductance map<sup>5</sup>. The nature and the origin of the LDOS modulations, in particular the short coherence length and the role of dopants<sup>6,7</sup>, are unclear at present. Several inhomogeneous electronic states have been proposed theoretically, including pair density waves<sup>8,9</sup>; hole Wigner crystal<sup>10</sup>; a Wigner crystal of hole pairs embedded in a d-wave resonating valence bond (RVB) state<sup>11</sup>; and valence-bond solid with or without charge order<sup>12</sup>. How certain inhomogeneous electronic states with CB order arise from the microscopic  $t$ - $J$  model of doped Mott insulators is the focus of this work. Recent density matrix renormalization group calculations performed on small  $t$ - $J$  clusters found approximate CB like patterns with strong one-dimensional stripe characters<sup>13</sup>. In this paper, we discuss a spatially unrestricted Gutzwiller approximation, which allows us to study large systems in the thermodynamic limit. We focus primarily on inhomogeneous solutions in the nonsuperconducting phase at moderate doping where the underlying homogeneous phase exhibits a Fermi surface (FS). Specifically, we consider the two situations displayed in Fig. 1 for the spectral intensity of the low energy single-particle excitations as measured by angle-resolved photoemission (ARPES), in the staggered flux phase (SFP)<sup>14</sup> and the uniform short-range RVB state<sup>15</sup> with realistic band parameters. The quasiparticle scattering in the SFP (Case A in Fig.1a) is dominated by the wave vector  $\mathbf{q}^*$  connecting the tips of the Fermi pock-

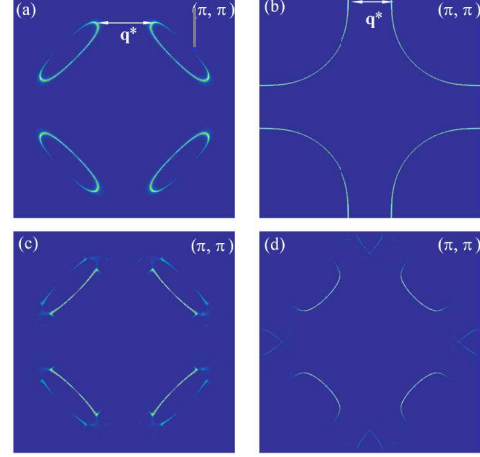


FIG. 1: Spectral intensity near the Fermi level in the SFP (a) and the Fermi liquid phase with realistic band parameters (b) in the  $t$ - $J$  model. Those in the corresponding checkerboard ordered states are shown in (c) and (d) where sections of the FS with high spectral intensity connected by  $\mathbf{q}^*$  are gapped.

ets with high spectral intensity. In Fig. 1b (Case B), the sections of the large FS around  $(\pm\pi, 0)$  and  $(0, \pm\pi)$  are nested and scattering by the nesting vector  $\mathbf{q}^*$  is enhanced. In both cases, the wave vector dependent susceptibility exhibits sharp peaks at  $\mathbf{q}^*$  and the system is prone to superlattice instabilities, akin to the examples discussed by Lomer<sup>16</sup>, and Rice and Scott<sup>17</sup> for two-dimensional band structures with nesting and saddle-points respectively. We show that this indeed happens in both cases, leading to inhomogeneous CB ordered states that are lower in energy than the uniform state. The resulting spectral intensity maps are shown in Figs. 1c and 1d where FS sections connected by  $\mathbf{q}^*$  are truncated. In Case A, the CB order is a secondary instability of the SFP that already exhibits a pseudogap in the LDOS. Case B, however, is more significant. The CB order produces a pseudogap around  $(\pm\pi, 0)$  and  $(0, \pm\pi)$ , the antinodes of the d-wave pairing gap function, leaving behind only “Fermi Arcs”, in agreement with ARPES experiments<sup>18</sup>.

In the Gutzwiller approximation, the projection of double-occupation from the Hilbert space is partially accounted for by the statistical weight factors,  $g^t$  and  $g^J$

multiplying the quantum coherent states connected by the hopping and the exchange processes<sup>19</sup>. The latter lead to renormalizations of the hopping and exchange parameters. The renormalized  $t$ - $J$  model can be studied by decoupling the exchange term

$$\begin{aligned}
H = & - \sum_{i < j, \sigma} g_{ij}^t t_{ij} \left( c_{i\sigma}^\dagger c_{j\sigma} + h.c. \right) - \mu \sum_{i, \sigma} c_{i\sigma}^\dagger c_{i\sigma} \\
& - \frac{3}{8} J \sum_{\langle i, j \rangle} g_{ij}^J \left( \sum_{\sigma} \chi_{ij}^* c_{i\sigma}^\dagger c_{i\sigma} + h.c. - |\chi_{ij}|^2 \right) \\
& - \frac{3}{8} J \sum_{\langle i, j \rangle} g_{ij}^J \left[ \Delta_{ij}^* (c_{i\uparrow} c_{j\downarrow} - c_{i\downarrow} c_{j\uparrow}) + h.c. - |\Delta_{ij}|^2 \right] \\
& + \sum_i \varepsilon_i \left( \sum_{\sigma} c_{i\sigma}^\dagger c_{i\sigma} + x_i - 1 \right). \quad (1)
\end{aligned}$$

Here  $\mu$  is the chemical potential,  $\chi_{ij} = \sum_{\sigma} \langle c_{i\sigma}^\dagger c_{j\sigma} \rangle$  and  $\Delta_{ij} = \langle c_{i\uparrow} c_{j\downarrow} - c_{i\downarrow} c_{j\uparrow} \rangle$  are the nearest neighbor bond and flux, and pairing fields, and  $t_{ij}$  is the hopping between sites  $i$  and  $j$ .  $t_{ij} = t$  between nearest neighbors (NN);  $t'$  for next NN. In the last line of Eq. (1),  $x_i = 1 - \sum_{\sigma} \langle c_{i\sigma}^\dagger c_{i\sigma} \rangle$  denotes the doped hole density at site  $i$ , and the averaged doping is given by  $\delta = (1/N_s) \sum_i x_i$  on a lattice of  $N_s$  sites.

There are two new features in the unrestricted Gutzwiller approximation. First, the usual Gutzwiller factors<sup>19</sup> now depend on the local hole density,

$$g_{ij}^t = \sqrt{\frac{4x_i x_j}{(1+x_i)(1+x_j)}}, \quad g_{ij}^J = \frac{4}{(1+x_i)(1+x_j)}. \quad (2)$$

In essence, the local doping concentration  $x_i$  is promoted to a variational parameter<sup>6</sup>. Second, as an electron hops between sites, the renormalized bandwidth will change by  $\mathcal{O}(1/N_s)$ . However, the kinetic energy of the occupied states changes by an amount of order unity, and this energy difference must be reflected in the equilibrium condition by the local fugacity  $\varepsilon_i$  in the last term of Eq. (1). The value of  $\varepsilon_i$  is determined by minimizing the energy with respect to  $x_i$ ,

$$\varepsilon_i = \sum_j \left[ 2t_{ij} \frac{\partial g_{ij}^t}{\partial x_i} \text{Re}(\chi_{ij}) + \frac{3J}{8} \frac{\partial g_{ij}^J}{\partial x_i} (|\chi_{ij}|^2 + |\Delta_{ij}|^2) \right].$$

In the rest of the paper, we focus on the normal state unless otherwise noted.

*Checkerboard order in the SFP* We choose  $t = 3J$  and set  $t'$  and further neighbor hopping to zero. In this case, the uniform normal state of Eq. (1) is the SFP for small to moderate doping. The spectral intensity near the Fermi level is shown in Fig. 1a for  $\delta = 0.102$ . To locate the wave vectors at which Lomer-Rice-Scott instabilities may occur, we calculate the static susceptibilities

$$\chi_{\alpha\beta}(q) = \sum_{k\sigma, mn} \Lambda_{\alpha}^{mn}(k, q) \Lambda_{\beta}^{nm}(k, -q) \frac{f(E_k^m) - f(E_{k+q}^n)}{E_{k+q}^n - E_k^m}$$

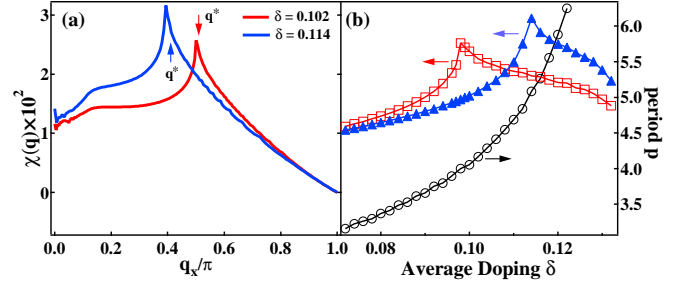


FIG. 2: (a) Susceptibility in the SFP in the density-bond channel along  $(q_x, 0)$ . The peak positions correspond to  $\mathbf{q}^* = (2\pi/4, 0)$ ,  $\mathbf{q}^* = (2\pi/5, 0)$  for the two doping levels. (b) Density-bond susceptibility at fixed  $\mathbf{q}^* = (2\pi/4, 0)$  (squares) and  $(2\pi/5, 0)$  (triangles) as a function of doping. Also shown is the doping dependence of inhomogeneity period  $p = 2\pi/q_x^*$  (circles).

where  $\Lambda_{\alpha}^{mn}(k, q)$  is the coupling vertex in the density, bond, and flux channels labeled by  $\alpha$ ,  $E_k^n$  is the quasi-particle band dispersion<sup>20</sup>. We find that all susceptibilities exhibit peaks at  $\mathbf{q}^* = (q_x^*, 0), (0, q_x^*)$ . The dominant density-bond ( $x$ -direction) susceptibility is plotted in Fig. 2a along  $(q_x, 0)$ . The  $\mathbf{q}^*$  can be identified by the location of the sharp peak and is doping-dependent and incommensurate in general. If an instability occurs at  $\mathbf{q}^*$ , the ground state will exhibit CB order with a periodicity  $p = 2\pi/q_x^*$ , which is shown in Fig. 2b, as a function of doping. Note that the maximum periodicity is limited by the stability of the SFP. For our parameters,  $p$  varies continuously between 4 and 5 in the doping range of 10 – 12%. To search for a spatially unrestricted Gutzwiller solution that allows static order at  $\mathbf{q}^*$  in finite systems, it is advantageous to study doping levels at which  $\mathbf{q}^*$  takes on commensurate values. In Fig. 2b, the susceptibility at fixed  $\mathbf{q}^* = (2\pi/4, 0)$  and  $(2\pi/5, 0)$  are shown as a function of doping. The peak structures allow the choice of doping to be made. We thus focused on an average doping  $\delta = 0.102$  where  $\mathbf{q}^*$  is consistent with an instability toward  $p = 4$  CB order.

We next study spatially unrestricted solutions on  $80 \times 80$  systems with  $4 \times 4$  and  $8 \times 8$  supercells wherein the  $x_i$ ,  $\varepsilon_i$ , and  $\chi_{ij}$  are allowed to have spatial variations. Their values are determined by the standard iterative solutions of the self-consistency equations. An additional four-fold symmetry may be enforced to reduce the number of variational degrees of freedom for faster convergence. Remarkably, the self-consistent state with  $p = 4$  CB order emerges with a significantly lower energy compared to the uniform SFP state. The real space CB patterns of local doping  $x_i$ , staggered plaquette flux  $(-1)^i \sum_{\square} \chi_{ij}''$ , valence bond  $\chi'_{i, i+\hat{x}}$ , and integrated LDOS are shown in Fig. 3 (a-d). Their Fourier transforms show dominant peaks at  $\mathbf{q}^* = (\pm 2\pi/4, 0), (0, \pm 2\pi/4)$ . The relative modulations in the CB state and the energy comparison to the uniform state are summarized in Table I. Interestingly, the charge density variations are small (less than

2%) while the bond and the plaquette flux variations are more significant. The flux and bond density wave instabilities in the SFP of the  $t$ - $J$  model were first revealed in the slave boson large- $N$  theory<sup>20</sup>. These results show that weak charge order in the SFP is a byproduct of the driving CB order of the valence bond and the plaquette flux. The accompanying weak charge ordering is in line with STM observations in Na-CCOC<sup>4</sup>.

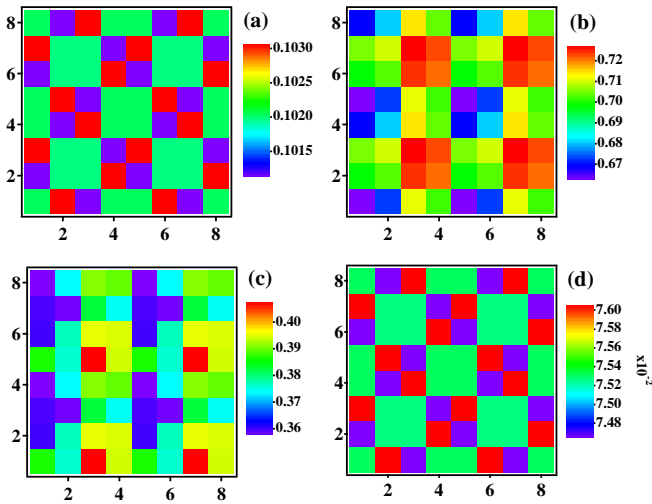


FIG. 3: 2D maps of (a) local doping concentration, (b) staggered plaquette flux, (c)  $x$ -direction bond, and (d) integrated local density of states.

It is important to note that the appearance of the local fugacity  $\varepsilon_i$  in Eq. (1) is essential for the emergence of the CB state with lower energy than its uniform counterpart. Indeed, without  $\varepsilon_i$ , a much more inhomogeneous state can emerge as a self-consistent solution<sup>21</sup>, but its energy is significantly higher than the uniform state (see Table I).

TABLE I: Modulation amplitudes and the energy of the  $4 \times 4$  and the  $5 \times 5$  checkerboard states emerging from the SFP and the Fermi liquid state.

	$x$ (%)	bond (%)	flux (%)	$E_0 - E_{\text{uniform}}(\%)$
$4 \times 4$	1.87	12.7	8.76	-1.22
$5 \times 5$	25.9	155	/	-0.167
Ref. <sup>21</sup>	62.4	35.6	94.7	0.347

The projected spectral function in the Gutzwiller approximation is given by  $A(i, j, \omega) = -2\text{Im}g_{ij}^t G(i, j, \omega + i0^+)$ , where  $G$  is the real-space retarded Green's function. The Gutzwiller factor arises from projecting the matrix elements of the electron operator between ground and excited states. The spectral intensity at the Fermi level  $A(k, \omega \simeq 0)$  maps out the FS shown in Fig. 1c. The  $4 \times 4$  checkerboard order opens and gaps out the tips of the Fermi pockets. The intensity is dominated by the inner branch of the remaining segments due to the anisotropy in the SFP coherence factors. Fine structures due to zone

folding and higher order scattering effects become visible only after the intensity scale is reduced by four orders of magnitude. In Fig. 4a, the band dispersion  $E(k)$  extracted from the quasiparticle peaks in  $A(k, \omega)$  is shown. It retains the general structure of the SFP, exhibiting a pseudogap in the LDOS  $\rho(r, \omega) = \sum_k e^{ikr} A(k, \omega)$  shown in Fig. 4b. The particle-hole asymmetry is much enhanced at these parameters. The checkerboard order induces a small energy gap at  $E_F$  in the dispersion along the  $M$ - $X$  direction, which is reflected in the additional dip in the LDOS at the Fermi level. It is worth pointing out that the suppression of the LDOS is particle-hole asymmetric and predominately resides on the occupied side.

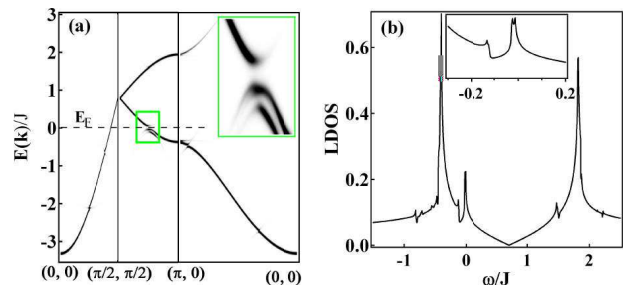


FIG. 4: (a) Quasiparticle dispersion in the checkerboard SFP. Inset shows the gap near the FS. (b) LDOS site (1, 1). Inset shows the LDOS near Fermi energy.

*Checkerboard order with realistic band dispersion* Next we examine whether the CB state emerges in the  $t$ - $J$  model with further neighbor hopping capable of producing the dispersion and the FS observed by ARPES<sup>22</sup>. The hopping integrals in Eq. (1) are chosen to be 6.0, -2.0, 0.71, 0.7, -0.41, 0.07 in units of  $J$  from the nearest up to the sixth neighbors respectively. The corresponding FS in the uniform Fermi liquid was shown in Fig. 1b at doping  $\delta = 0.11$ . It reveals the partially nested segments near  $(\pm\pi, 0)$  and  $(0, \pm\pi)$  with nesting vectors  $\mathbf{q}^* \simeq (\pm 2\pi/5, 0), (0, \pm 2\pi/5)$ . The set of parameters is chosen such that the nesting properties in the realistic band dispersion are most pronounced at low dopings. Similar to the SFP, the calculated static, wave vector dependent susceptibilities peak at these nesting vectors and are most pronounced in the density-bond channel. Fig. 5a displays the (logarithmic) divergence as  $\mathbf{q} \rightarrow \mathbf{q}^*$ , indicating possible instabilities toward spatially inhomogeneous states. On  $80 \times 80$  systems with  $10 \times 10$  supercells, we find that the spatially unrestricted solution converges to the CB state with  $p = 5$ , consistent with the nesting vector  $\mathbf{q}^*$ . The  $5 \times 5$  pattern is shown in Fig. 5b for the doping concentration. The amplitudes of the variations in doping and bond (Table I) are significantly larger than in the SFP owing to the more singular behavior of the susceptibility. The quasiparticle dispersion obtained from the calculated  $A(k, \omega)$  near the Fermi level is shown in Fig. 5c. The CB order opens up a sizable gap near  $(\pm\pi, 0), (0, \pm\pi)$  and truncates the nested

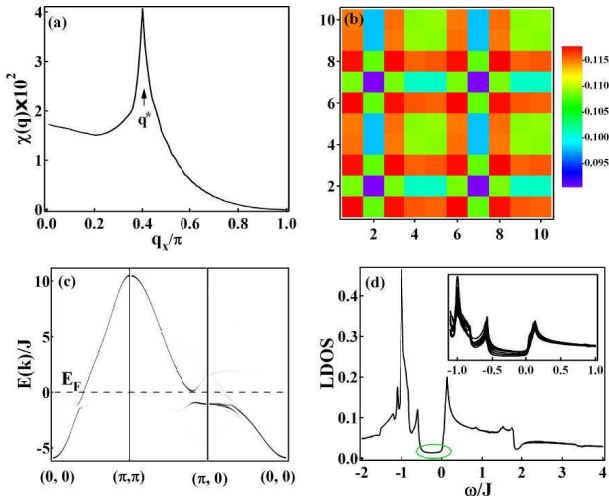


FIG. 5: (a) Density-bond susceptibility along  $(q_x, 0)$ . (b) 2D map of the local doping showing  $5a \times 5a$  order. (c) Quasi-particle dispersion. (d) Tunneling LDOS. The circle marks the gap opening just below the Fermi level. Inset shows the spectra near Fermi level at all different sites.

segments of the original FS as shown in Fig. 1d.

The gap near the antinodes and the residual Fermi arcs around the nodes are reminiscent of the pseudogap phenomenology observed by ARPES<sup>23</sup>. It is important to point out the differences between the CB order induced pseudogap and one that is due to a d-wave pairing gap. A finite zero-bias conductance must remain due to the finite “volume” of the residual Fermi arcs, whereas a d-wave pairing gap leads to a linearly vanishing LDOS. In Fig. 5d, the calculated  $\rho(r, \omega)$  in the  $p = 5$  CB state is shown. The gap opening pushes the van Hove peak downward, resulting in a substantial lowering of the kinetic energy. However, the gap opens predominantly on the occupied side leaving the spectrum particle-hole asymmetric even at low energies. We find that this feature, also observed in the inhomogeneous SFP in Fig. 4b, is

rather generic of the CB ordered states associated with the partial gapping of the FS. This is in contrast to the particle-hole symmetric LDOS in a pairing-induced pseudogap state and the conventional charge density wave state with a fully gapped FS. A direct comparison to the STM spectra in oxchlorides<sup>4</sup> is difficult since the correlation length of the observed CB pattern is very short (20a), although particle-hole asymmetry in the tunneling spectra is apparent.

In conclusion, we have shown that  $pa \times pa$  ordered states emerge in the  $t$ - $J$  model from both the SFP and the Fermi liquid phase with realistic band parameters for the cuprates. The CB states we found originate from a generally incommensurate partial FS instability of the Lomer-Rice-Scott variety, and are different from the bond-ordered states<sup>12</sup> inherent of the spin-Pierls or dimerized spin liquids at half-filling. As such, the inhomogeneous states found in the unrestricted Gutzwiller approximation are expected to be robust against Gutzwiller projection of double occupation. We have tested that the CB state is stable in the presence of a weak pairing order parameter and long-range Coulomb interaction. However, in the parameter regime investigated, the uniform d-wave superconducting state always has a lower energy. Thus, the CB ordered state cannot coexist with d-wave pairing well inside the superconducting phase where the FS has been gapped out except for point zeros (nodes). Due to such competitions, the CB order discussed here may arise in the cuprates only in the pseudogap regime or close to the superconducting phase boundary, and may manifest in the form of fluctuating order pinned by dopant disorder. Finally, the NN Coulomb interaction  $V$  in the  $t$ - $J$ - $V$  model, which is known to reduce the  $d$ -wave pairing strength while enhancing that of the valence bond,<sup>24</sup> may lead to the coexistence of CB order and  $d$ -wave superconductivity.

We thank H. Ding, D.-H. Lee, and P.A. Lee for useful discussions. This work is supported by DOE grant DE-FG02-99ER45747 and ACS grant 39498-AC5M.

- <sup>1</sup> J.E. Hoffman, et. al. Science **295**, 466 (2002).
- <sup>2</sup> C. Howald, et. al. Phys. Rev. B **67**, 014533 (2003).
- <sup>3</sup> M. Vershinin, et. al. Science **303**, 1995 (2003).
- <sup>4</sup> T. Hanaguri, et. al., Nature **430**, 1001 (2004).
- <sup>5</sup> K. McElroy, et. al. Phys. Rev. Lett. **94**, 197005 (2005).
- <sup>6</sup> Z. Wang, et. al. Phys. Rev. B **65**, 064509 (2002).
- <sup>7</sup> T.M. Rice and H.Tsunetsugu, cond-mat/0509382 (2005).
- <sup>8</sup> H.-D. Chen, et. al. Phys. Rev. Lett. **93**, 187002 (2004).
- <sup>9</sup> Z. Tesaonovic, Phys. Rev. Lett. **93**, 217004 (2004).
- <sup>10</sup> H.C. Fu, J.C. Davis, and D.-H. Lee, cond-mat/0403001.
- <sup>11</sup> P.W. Anderson, cond-mat/0406038 (2004).
- <sup>12</sup> M. Vojta, Phys. Rev. B **66**, 104505 (2002); M. Vojta, Y. Zhang, and S. Sachdev, Phys. Rev. B **62**, 6721 (2000).
- <sup>13</sup> S.R. White and D.J. Scalapino, Phys. Rev. B **70**, 220506 (2004).
- <sup>14</sup> I. Affleck and J.B. Marston, Phys. Rev. B **37**, 3774 (1988);

- G. Kotliar, Phys. Rev. B **37**, 3664 (1988).
- <sup>15</sup> M. Grilli and G. Kotliar, Phys. Rev. Lett. **64**, 1170 (1990).
- <sup>16</sup> W.M. Lomer, Proc. Phys. Soc., London **80**, 489 (1962).
- <sup>17</sup> T.M. Rice and G.K. Scott, Phys. Rev. Lett. **35**, 120 (1975).
- <sup>18</sup> M.R. Norman et. al. Nature **392**, 157 (1998); K.M. Shen, et. al. Science **307**, 901 (2005); U. Chatterjee, et. al. cond-mat/0505296.
- <sup>19</sup> F.C. Zhang, et. al. Supercond. Sci. Tech. **1**, 36 (1988).
- <sup>20</sup> Z. Wang, G. Kotliar, and X.F. Wang, Phys. Rev. B **42**, 8690 (1990); D.C. Morse and T.C. Lubensky, Phys. Rev. B **43**, 10436 (1991).
- <sup>21</sup> D. Poilblanc, Phys. Rev. B **72**, 060508(R) (2005).
- <sup>22</sup> M.R. Norman and H. Ding, Phys. Rev. B **57**, 11089 (1998).
- <sup>23</sup> H. Ding, et.al. Nature **382**, 51 (1996); A.G. Loeser, Science **273**, 325 (1996).
- <sup>24</sup> S. Zhou and Z. Wang, Phys. Rev. B **70**, 020501(R) (2004).

